Top Catal (2016) 59:278–291
DOI 10.1007/s11244-015-0447-0

ORIGINAL PAPER

Mesopore-Modified SAPO-18 with Potential Use as Catalyst for the MTO Reaction

Teresa Álvaro-Muñoz[1] · Carlos Márquez-Álvarez[1] · Enrique Sastre[1]

Published online: 7 August 2015

Abstract SAPO-34 silicoaluminophosphates are well known as catalysts for the synthesis of light olefins–ethylene and propylene–from methanol by using the methanol to olefins (MTO) process, first described by Mobil. SAPO-18, which has a microporous framework structure related to but crystallographically distinct from SAPO-34, has been much less studied but promises to be a potential catalyst in the MTO process. The main drawback of these catalysts in this reaction is their rapid deactivation, due to the deposition of heavy carbonaceous products–coke–on the surface of the solid avoiding the access of methanol molecules to the active centres located inside the pores of the SAPO catalysts. We have used different mesoporogen agents–nanoparticulate carbons and chitosan–aiming to generate mesoporosity in the SAPO-18 crystals, in an attempt to improve the accessibility of the reagent to the active centres of SAPO-18 and, in that way, inhibit catalyst deactivation. All the materials prepared in this work present similar framework composition and silicon distribution and the main difference among them is the hierarchical porosity generated by the mesoporogen additives use in the synthesis, as determined by STEM. Using chitosan polymer as a secondary template results in an increase of the external surface, which improved significantly the internal diffusivity enhancing the life time of the catalyst in the MTO process.

Keywords AEI structure · Silicoaluminophosphate · Mesoporous SAPO-18 · Hierarchical microporous materials · Short chain olefins · MTO

1 Introduction

Light olefins, which are conventionally produced by thermal cracking of naphtha, are key components in the petrochemical industry that will probably play an important role in any future methanol-based chemicals economy. Methanol can be efficiently produced from syngas obtained by natural gas reforming or carbon gasification, but also through carbon neutral routes [1] such as chemical recycling of carbon dioxide via hydrogenation [2] or from syngas obtained by biomass gasification [3]. Mobil's process for the conversion of methanol to gasoline (MTG) provided a new route for the conversion of natural gas or coal to gasoline [4–7]. The importance of light olefins as intermediates in the conversion of methanol to gasoline has prompted several studies on methods for selectively producing them from methanol on zeolite catalysts. The methanol to olefins (MTO) process could be considered as the first step in the MTG process. The primary products formed from oxygenates are light olefins (ethylene, propylene and butenes) and the secondary products are heavier hydrocarbons, corresponding to the gasoline fraction (C5–C10). Some years ago, numerous studies aimed at increasing the selectivity to light olefins on catalysts based on modified HZSM-5 zeolites were published. The concentration of strong acid sites, responsible of hydrogen transfer reactions, was identified as the key factor in the production of gasoline from the initial short chain olefins produced. So, decreasing the acidity of the ZSM-5 catalysts (number and strength of the acid centres) leads to an

Electronic supplementary material The online version of this article (doi:10.1007/s11244-015-0447-0) contains supplementary material, which is available to authorized users.

✉ Teresa Álvaro-Muñoz
teresa.alvaro@icp.csic.es

[1] Instituto de Catálisis y Petroleoquímica, ICP-CSIC, C/Marie Curie, 2, 28049 Madrid, Spain

enhanced selectivity towards light olefins [8–15]. The development of silicoaluminophosphate (SAPO) molecular sieves with microporous framework structures opened other interesting perspectives [16]. SAPO materials possess acid sites of medium strength and, therefore, they presented a very interesting alternative to obtain high selectivity towards light olefins in the MTO process. Most of the studies reported hitherto have been mainly focused on the SAPO-34 type material (isomorphous to chabazite), which allows for carrying out different modifications in its preparation and composition [17–23]. Zeolite-type small-pore microporous SAPO-34 has been proven an excellent catalyst for the MTO process, showing exceptionally high selectivity to lower olefins, with reported selectivities to C2–C4 olefins over 80 % [24–28].

SAPO-18 is a silicoaluminophosphate structurally related to chabazite [29, 30]. The pore structure of both materials presents large cavities interconnected through windows with the same dimensions (circular 8-rings with 3.8 Å diameter). These supercages are formed between alternate layers of double six-membered rings parallel to the *ab* plane hexagonal prisms that, in SAPO-34, are related by a simple translation and therefore have the same orientation, while, in SAPO-18, are related by a *c*-glide, which causes the supercage to have a pear like shape (Fig. 1). Due to the close structural relationship between both materials, SAPO-18 and SAPO-34 show similar behaviour in the MTO process [31–33]. However, in spite of the good activity and high selectivity towards light olefins of these catalysts in the MTO transformation, the main drawback under reaction conditions is their rapid deactivation. Deactivation starts when aromatics and heavy branched hydrocarbons are formed inside the large cages. These molecules cannot diffuse though the porous structure of the catalyst because their kinetic diameter is larger than the pore openings. Therefore, they remain inside the cages where they can form carbonaceous deposits that block the cage windows and prevent the access of molecules to the active sites [18, 34, 35]. Various strategies have been developed trying to solve this problem. The challenge is to improve the accessibility of the active sites without changing their properties. This can be accomplished during or after the synthesis of the zeolitic material, introducing mesopores in the zeolite crystals, synthesizing zeolitic materials in nanoscale dimensions or using a support of a mesoporous material in which the zeolite is deposited. Intracrystalline mesoporosity can be introduced by different approaches, usually by dealumination [36, 37] or desilication [36–39] that lead to partial disintegration of the zeolite crystal changing the number and the strength of the acid sites of the original material. The second approach is based on crystallization of the zeolite in the presence of an auxiliary mesoporogen template that could be easily removed after the crystallization [40, 41].

Creation of mesopores in SAPO crystals would enhance diffusion of products and prevent secondary reactions, thus improving the catalyst life time. It has been shown that carbon templating provides a successful strategy to synthesize mesopore-modified zeolites [41]. Addition of carbon black to the synthesis gels allowed obtaining zeolite crystals with embedded carbon particles, which created intracrystalline mesopores once removed by combustion. This carbon-templating approach to mesoporous zeolites was first reported by Jacobsen et al. [41]. This strategy consists of impregnating a carbon source with a zeolite precursor solution which promotes the nucleation of the

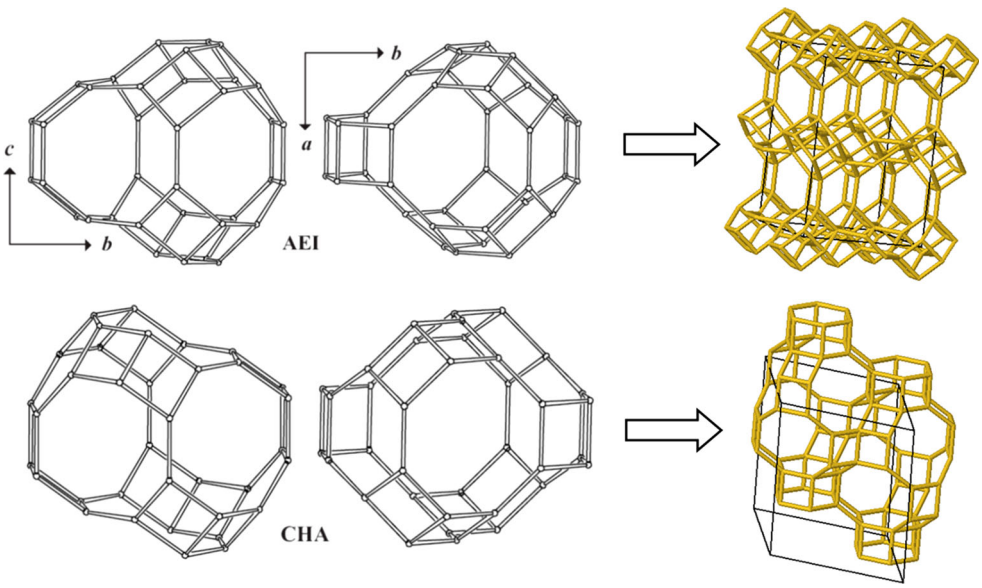

Fig. 1 Cage structures of SAPO-34 and SAPO-18 [64]

zeolite crystals around the carbon material. In this manner, the zeolite crystals grow and partially encapsulate the carbon. During the calcination, the carbon is burned off, which results in the generation of intracrystalline mesopores. So far, the carbon-templating method has been used to prepare different zeolites, including ZSM-5 [41], ZSM-11 [42], ZSM-12 [43, 44], zeolite Y [45] and zeolite beta [46], and it is also possible to synthesize mesoporous zeotypes, such as AlPOs and SAPOs [46–48]. Recently, we have applied this strategy to obtain mesoporous SAPO-34. It was found that using these additives pore volume increased which improved significantly the internal diffusivity of these materials. These mesopore-modified SAPOs were tested in the MTO reaction exhibiting an improved conversion of methanol to light olefins compared with the conventional material.

In this work, we explore the carbon templated synthesis approach to obtain mesopore-modified SAPO-18 crystals, and evaluate its effect on the catalytic behaviour in the MTO reaction. Due to the higher polarity of the aluminophosphate framework as compared to zeolites, pre-treatment of the carbon template with concentrated nitric acid was carried out aiming to create surface oxygen functionalities and increase its affinity with the SAPO crystals. Additionally, we tested as mesoporogen template a hydrophilic polymer, namely chitosan, a commercially available low cost biopolymer, which is obtained by partial deacetylation of chitin extracted from the shells of crustaceans. Chitosan has been used as additive in the sol–gel synthesis of silica, alumina and aluminosilicates, and has proven to act as mesoporosity generator and structural stabilizer, leading to materials with high surface area and large pore volume [49–52]. We envisaged that chitosan might exhibit higher affinity with the polar SAPO framework than hydrophobic carbon particles and would, therefore, be also an efficient mesoporogen agent for SAPO materials.

2 Experimental

2.1 Synthesis of SAPO-18 Molecular Sieves

Hydrothermal synthesis of SAPO-18 samples was carried out at 433 K from gels with the following molar composition, using *N*,*N*-diisopropylethylamine (DPREt) as template:

1 Al_2O_3:0.8 P_2O_5:0.6 SiO_2:1.6 DPREt:25 H_2O

Hydrated aluminium hydroxide (Sigma Aldrich, 100 %), 85 % phosphoric acid (Riedel-de Haën) and fumed silica (Aerosil, Degussa) were used as sources of the framework elements. The same silicon to aluminium atomic ratio (Si/Al = 0.3) was used for all the synthesis gels. In a typical synthesis, aluminium hydroxide was added slowly to a 6.8 M phosphoric acid aqueous solution and the mixture was stirred for 2 h to form a uniform gel. Fumed silica was then added to this mixture followed by addition of the DPREt template. The resulting gels were transferred into Teflon-lined stainless steel autoclaves with a capacity of 40 cm^3, which were heated statically at 433 K under autogenous pressure for 6 days. The resulting solids were collected by filtration, washed with water and ethanol and dried at room temperature overnight. Different mesoporogen agents were added to the synthesis gels prior to hydrothermal treatment as indicated below. For comparative purposes, a reference material was synthesized without any mesoporogen agent. The synthesis conditions for the different samples are summarized in Table 1.

The organic template, the mesoporogen agents and the water trapped within the micropores of the as-synthesized solids were removed by calcination at 823 K prior to catalyst testing. Complete removal of the organic compounds was assessed by TGA.

2.1.1 Mesoporous Zeotypes with Carbon Black Particles

For the synthesis of mesoporous zeotypes, carbon black particles (BP-2000 from Cabot Corporation) as-received (CB2000) or pre-treated with concentrated nitric acid (CB2000-OX) were added to the synthesis gels and the mixtures stirred for about 3 h before transferring to the autoclaves.

Pre-treatment of the carbon template with concentrated nitric acid was carried out aiming to create surface oxygen functionalities that would increase its affinity with the SAPO crystals. To do that, carbon particles were treated with concentrated (14 M) HNO_3 solution (100 mL/10 g of carbon) at boiling temperature for 10 min [53]. The resulting solid was collected by filtration, washed with distilled water until neutral pH and dried overnight at 373 K. In all cases, carbon particles were dried at 110 °C overnight prior to their use in the synthesis of SAPO-18.

Table 1 SAPO materials synthesized with different mesoporogen additives

Sample	Additive	wt% additive in the gel	Phase
S-18	–	–	AEI
C-18-1	CB2000	2.68	AEI
C-18-2	CB2000	4.25	AEI
C-18-1OX	CB2000-OX	2.68	AEI
C-18-2OX	CB2000-OX	4.25	AEI
CHI-18-1	Chitosan	1.50	AEI
CHI-18-2	Chitosan	2.00	AEI
CHI-18-3	Chitosan	4.90	AEI + AFI

2.1.2 Mesoporous Zeotypes with Chitosan

As chitosan is soluble only in acidic media, SAPO-18 synthesis gels containing this polymer were prepared by first adding slowly chitosan (medium molecular weight, 75–85 % deacetylated chitin from Sigma-Aldrich) to a diluted phosphoric acid solution under stirring. The mixture was stirred for 1 h to dissolve chitosan prior to addition of aluminium hydroxide and fumed silica.

2.2 Characterization

Powder X-ray diffraction (XRD) patterns of as-synthesized and calcined samples were recorded on a PANalytical X'Pert Pro diffractometer using CuK_α radiation with a nickel filter. Textural properties were determined by nitrogen adsorption/desorption measurements using a Micrometrics ASAP 2010 volumetric apparatus. Previous to measure the nitrogen adsorption/desorption isotherms, samples were degassed at 623 K under vacuum for at least 20 h. Total pore volume was determined at $P/P_0 = 0.975$. Surface area was determined by the BET method. Micropore volume and non-micropore or external surface area and volume were estimated by the t-plot method. The crystal size and morphology were examined by scanning electron microscopy (SEM) using a JEOL JSM 6400 or a Philips XL30 microscope, operating at 20 kV. Transmission electron microscopy (TEM) studies were carried out with a JEOL 2100F instrument using an acceleration voltage of 200 kV.

The organic content of the samples was determined by thermogravimetric analysis (TGA) using a Perkin-Elmer TGA7 instrument. TG analyses were carried out at a heating rate of 20 K/min under air flow. Chemical analysis of Al, P and Si in calcined samples was performed by inductively coupled plasma optical emission spectrometry (ICP-OES, Perkin-Elmer 3300DV instrument) after sample dissolution by alkaline fusion.

^{29}Si CP/MAS NMR spectra were recorded at room temperature using a Bruker AV-400-WB spectrometer operating at 79.5 MHz, with a 4 mm probe spinning at 10 kHz. A $\pi/2$ pulse of 3 μs, contact time of 6 ms and recycle delay of 5 s were used. The chemical shifts were referenced to tetramethylsilane (TMS), taken as 0 ppm.

Acidity measurements were carried out by ammonia temperature-programmed desorption (NH_3-TPD), using a Quantachrome ChemBET-3000 TPR/TPD equipment. Samples were pre-treated at 823 K for 1 h under helium flow (25 mL/min) and ammonia was adsorbed at 400 K by flowing a 5.0 vol% NH_3/He stream for 4 h at a rate of 15 mL/min. Weakly adsorbed NH_3 was removed under He flow (25 mL/min) at 400 K for 30 min and, finally, the temperature was increased to 823 K at a rate of 10 K/min.

2.3 Catalysts Testing

Methanol conversion to olefins was tested in a continuous, down flow, packed bed reactor fully automated and controlled from a personal computer (PID Eng&Tech Microactivity Reference), operating at atmospheric pressure. Catalyst weight (1.0 g; 20–30 mesh pellets size) and methanol flow rate (0.025 mL/min) were adjusted in order to obtain a weight hourly space velocity (WHSV) of 1.2 h^{-1}. Previous to the reaction, samples were pre-treated under nitrogen flow at 723 K for 1 h. During the reaction, nitrogen was used as an inert diluent gas and co-fed with methanol into the reactor with a constant methanol/nitrogen molar ratio of 1/1. The reaction products were analysed on-line by gas chromatography using a Varian CP3800 gas chromatograph equipped with flame ionization (FID) and thermal conductivity (TCD) detectors, with a Petrocol DH5 0.2 capillary column and a Porapack Q 80–100 mesh packed column for separation of hydrocarbons and oxygenates, respectively. Conversion was defined as the amount of methanol transformed to hydrocarbon products, thus considering the intermediate product dimethyl ether as unconverted methanol. Selectivities were calculated as molar percentage of every product in the mixture of hydrocarbons obtained.

3 Results and Discussion

3.1 Catalysts Characterization

The X-ray powder diffraction patterns of the as-synthesized samples (Fig. 2) are in good agreement with those reported earlier for SAPO-18 (framework code AEI) [29], except for the sample synthesized with the highest chitosan concentration (4.9 wt%) which showed additional peaks indicating the presence of the AFI phase (Table 1). XRD patterns of calcined samples show that all the materials maintain the AEI structure after calcination (Figure S1, Supplementary Information). However, it is remarkable that samples prepared with mesoporen agents show less intense diffraction patterns compared to the sample obtained without mesoporogen additives, which might be attributed to the presence of smaller crystalline domains in the former samples due to intracrystalline mesopores. The framework of this kind of material is very flexible [29, 54] so the unit cell dimensions show considerable changes from as-synthesized to calcined samples. These changes are reflected in some differences in the diffraction patterns after calcination.

In Fig. 3, SEM micrographs of different samples are presented, clearly showing the plate-like shape characteristic of the AEI crystallites, with sizes around

0.4 × 0.3 μm. The crystal size of the different materials is hardly influenced by the type of mesoporogen agent employed in the synthesis, although it can be seen that samples prepared with chitosan have a slightly smaller crystal size.

TGA were performed aiming to verify the incorporation of *N*,*N*-diisopropylethylamine and mesoporogen agents in the structure of the as-made samples and their subsequent complete elimination after calcination prior to the use of SAPO-18 materials in the catalytic reactions. The TGA profiles of the samples studied are plotted in Fig. 4. These profiles show four different weight loss steps (Table 2). The first weight loss (step I), at temperatures below 423 K, can be attributed to desorption of adsorbed water molecules. It should be noted that samples synthesized with the oxidized carbon template show significantly larger weight loss in this temperature range compared to the other samples. This could be attributed to the presence of a relatively high concentration of acidic groups on the surface of the modified carbon formed by treatment with concentrated nitric acid. These acidic groups would contribute to the adsorption of larger amount of water in the as-synthesized samples, which would result in higher weight loss in the first step of the thermograms. However, the acidic groups on the carbon surface are known to decompose at low

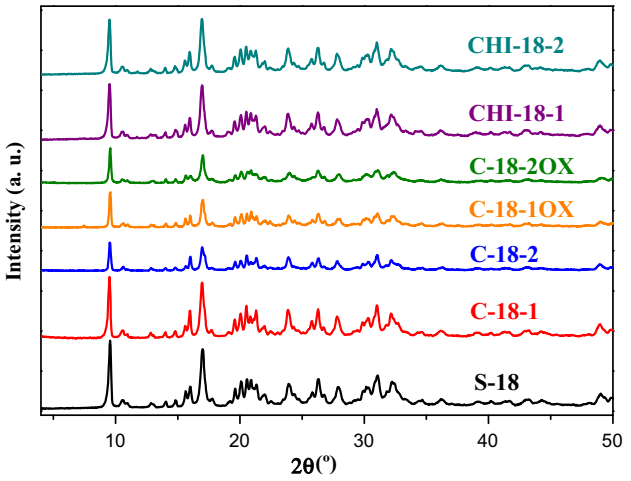

Fig. 2 X-ray diffraction patterns of as-syntehsized SAPO-18 materials

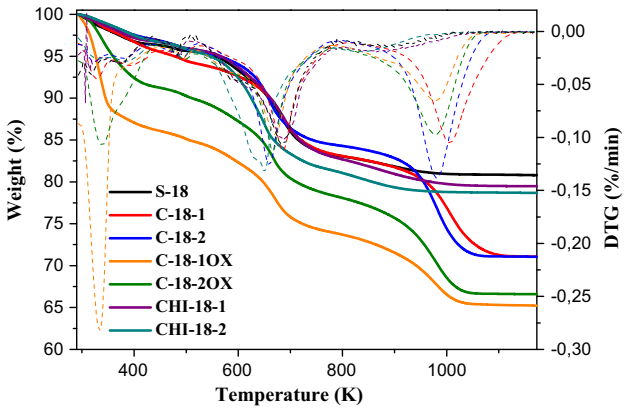

Fig. 4 Thermogravimetric analyses of SAPO-18 samples

Fig. 3 Scanning electron micrographs of calcined SAPO-18 samples

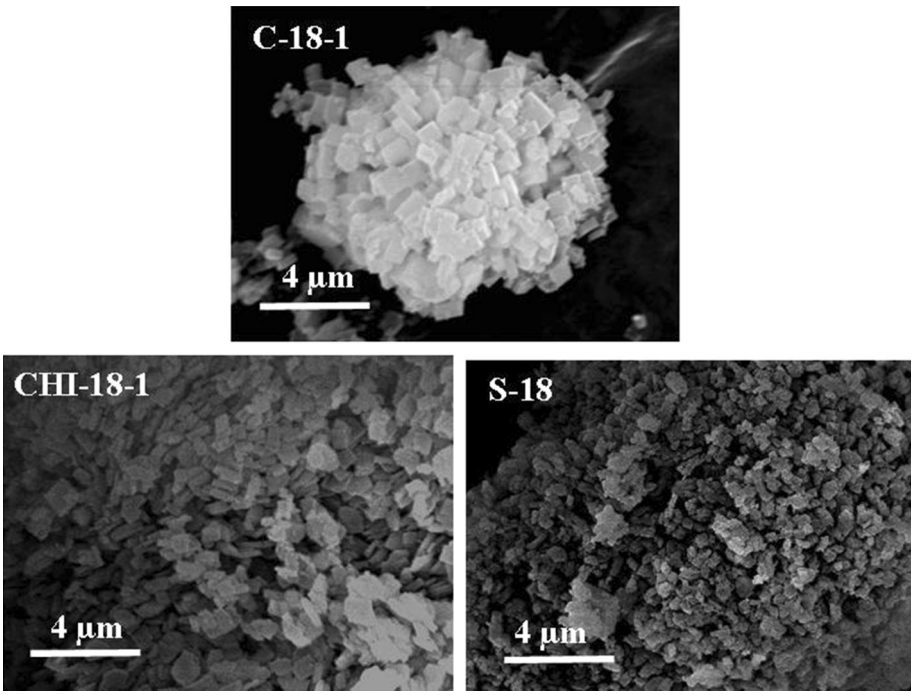

Table 2 Thermogravimetric analysis of the samples

Sample	Weight loss (%)			
	I (T < 423 K)	II (423 > T < 523 K)	III (523 > T < 823 K)	IV (T > 823 K)
S-18	3.6	0.8	12.6	2.3
C-18-1	4.6	1.5	11.0	11.8
C-18-2	2.9	1.5	11.2	13.3
C-18-1OX	13.7	1.6	10.7	8.6
C-18-2OX	8.5	1.4	11.5	11.7
CHI-18-1	3.2	0.9	13.2	3.2
CHI-18-2	3.3	1.2	14.0	2.8

temperatures releasing CO_2 and, therefore, it can be expected that decomposition of acidic groups also contributes to the weight loss observed for samples C-18-1OX and C-18-2OX at temperatures below 423 K. Between 423 and 473 K (step II), a characteristic weight loss typical of this kind of materials occurs, which is attributed to hydroxyl groups coordinated to aluminium atoms that are removed at higher temperature than physisorbed water. This process also occurs with other SAPOs [55]. Decomposition and combustion of the templates take place at higher temperatures, giving rise to two weight loss steps, one between 523 and 823 K (step III) and another at temperatures higher than 823 K (step IV). The later step shows a small weight loss for the samples obtained with chitosan and without mesoporogen agent that can be associated with the removal of organic residues occluded in the channels and cages of the SAPO-18. Therefore, the profiles for removal of chitosan and the amine template seem to overlap, which hinders a direct estimation of the amount of chitosan incorporated in the SAPO crystals. However, combustion of carbon black particles occurs at temperatures over 850 K. Hence, in the case of samples synthesized with carbon black, a significant weight loss takes place in step IV, mainly due to removal of carbon particles occluded within the SAPO-18 crystals. It can be observed that the weight loss of step IV (Table 2), and therefore the amount of carbon incorporated in the solid, increases with the amount of carbon added to the gel. However, the quantity of carbon trapped in the crystals was lower for samples prepared with acid pre-treated carbon (at a given carbon concentration in the synthesis gel). Thus, surface oxidation of carbon did not seem to produce the expected increase of affinity between carbon particles and the SAPO framework.

In Fig. 5, the nitrogen adsorption and desorption isotherms of selected materials after calcination of the templates and the mesoporogen additives are plotted. In Table 3, the calculated BET surface area, micropore surface area and volume and non-micropore (i.e., mesopore or external) surface area and volume of all samples are reported. Although it is commonly accepted that this

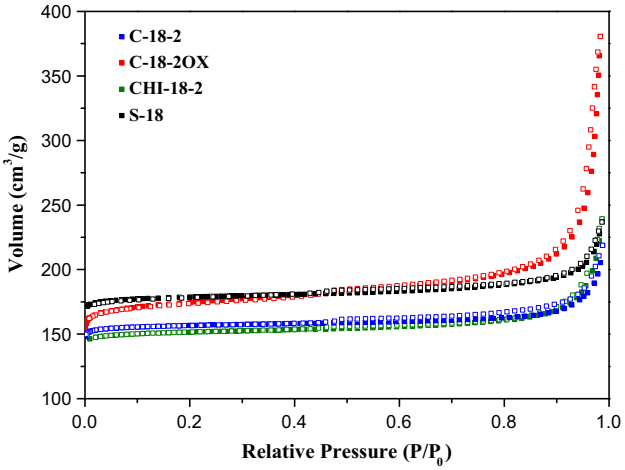

Fig. 5 Nitrogen adsorption–desorption isotherms of calcined SAPO-18 materials. *Full symbols* adsorption, *open symbols* desorption

technique is not the most appropriate way to determine unambiguously the surface and pore volume of small pore materials like SAPO-18, these data will be used for comparative purposes. It can be observed that all the materials synthesized with mesoporogen additives have lower values of micropore surface area and volume compared to the conventional SAPO-18 sample, and slightly higher non-micropore surface area and volume. Thus, inclusion of the mesoporogen templates led to a significant increase of the relative contribution of mesoporosity to the overall porosity of the samples. Similar behaviour has been described with other zeolites and SAPOs prepared with carbon [41, 43, 56, 57]. Samples prepared with carbon previously treated with acid possess higher values of non-micropore surface and volume than samples prepared with the unmodified carbon, despite the lower carbon content estimated by TGA for the former samples.

An important aspect to be discussed is the actual effect on accessibility of the micropores due to the mesopores created inside the crystals. In this sense, transmission electron microscopy of some samples has been realized. TEM micrographs of sample CHI-18-2 are shown in Fig. 6. Areas with lower contrast can be observed within the

Table 3 Textural properties of calcined SAPO-18 samples

Sample	Specific surface area (m^2/g)			Pore volume (cm^3/g)			
	S_{BET}	S_{micro}	S^a_{ext}	V_{tot}	V_{micro}	V^a_{ext}	V_{micro}/V_{total}
S-18	703	691	12	0.37	0.27	0.10	0.73
C-18-1	583	570	13	0.32	0.24	0.08	0.75
C-18-2	579	564	15	0.34	0.24	0.10	0.71
C-18-1OX	619	600	19	0.37	0.24	0.13	0.65
C-18-2OX	642	585	57	0.38	0.25	0.13	0.66
CHI-18-1	458	429	29	0.30	0.19	0.11	0.63
CHI-18-2	557	537	20	0.37	0.23	0.14	0.62

[a] Data on "external" surface area and pore volume refer to total non-micropore void space, combining both actual external surface of crystals and mesopores

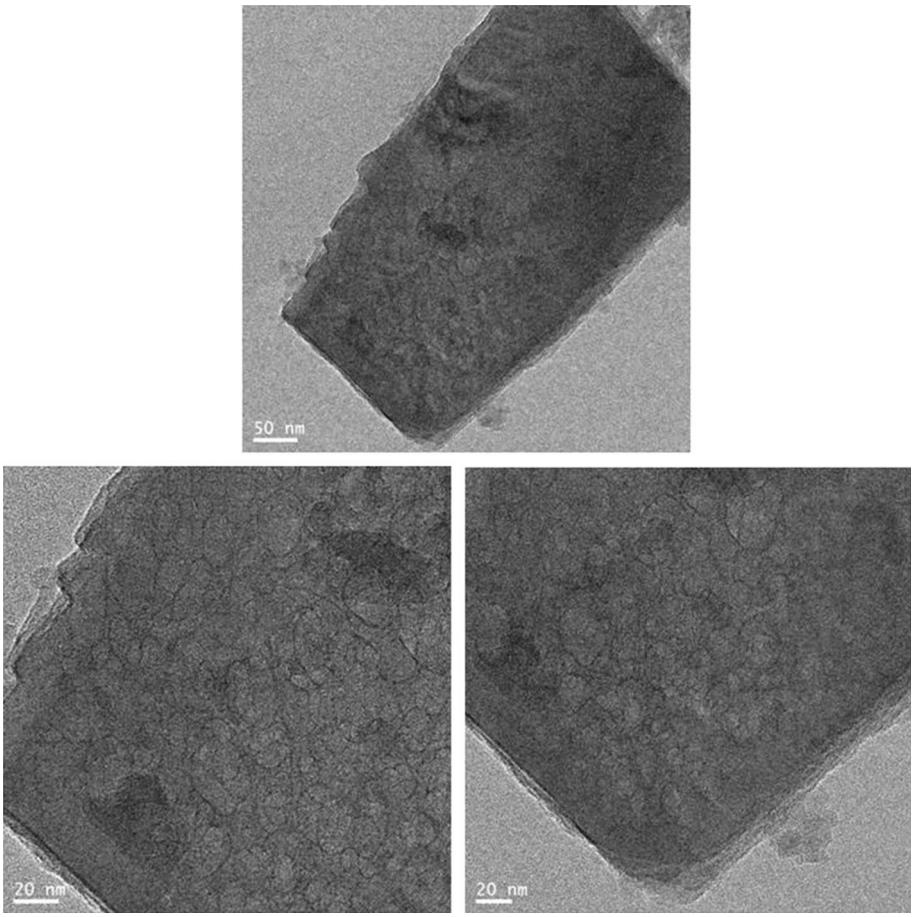

Fig. 6 TEM micrographs of the calcined sample CHI-18-2

crystals, showing the presence of mesopores with relatively uniform size around 10 nm in diameter. The presence of these cavities within the mesopore size range is more evident in the STEM micrographs shown in Fig. 7. However, as will be discussed below, the catalytic activity results suggest that the majority of the mesopore void space might not opened to the external surface of the crystals and, therefore, this mesoporosity would have a limited effect on the enhancement of accessibility to micropores.

The chemical composition obtained by ICP-OES is presented in Table 4. In all the samples, the Si/(Al + P) atomic ratio is close to that of the synthesis gel. The addition of mesoporogen agents to the synthesis gel has little effect on the chemical composition of the final inorganic framework. The incorporation of Si to the SAPO-18 framework has been studied by ^{29}Si MAS NMR (Fig. 8). All the spectra are quite similar and consist of a broad envelope in the −70 to −120 ppm range, corresponding to

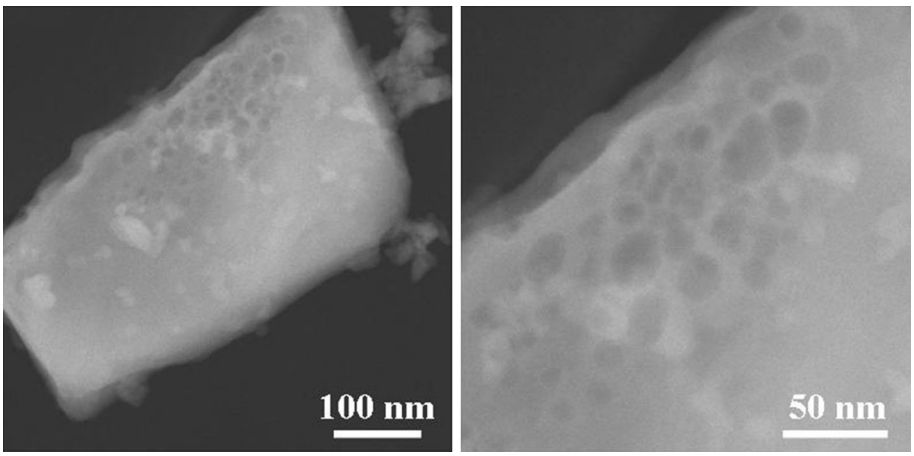

Fig. 7 STEM micrographs of the calcined sample CHI-18-2

Table 4 Chemical analyses and acid sites concentration of the materials synthesized from gels with atomic ratio Si/(Al + P) = 0.16

Sample	Molar composition	Si/(Al + P)	Si incorporation[a]	Acidity (mmol NH_3/g)[b]
S-18	$Si_{0.16}Al_{0.43}P_{0.41}O_2$	0.14	0.93	0.41
C-18-1	$Si_{0.14}Al_{0.44}P_{0.42}O_2$	0.16	1.03	0.42
C-18-2	$Si_{0.14}Al_{0.49}P_{0.37}O_2$	0.16	1.03	0.43
C-18-1OX	$Si_{0.12}Al_{0.47}P_{0.41}O_2$	0.14	0.88	0.38
C-18-2OX	$Si_{0.16}Al_{0.48}P_{0.36}O_2$	0.19	1.17	0.46
CHI-18-1	$Si_{0.15}Al_{0.45}P_{0.40}O_2$	0.18	1.08	0.47
CHI-18-2	$Si_{0.13}Al_{0.46}P_{0.41}O_2$	0.15	0.95	0.44

[a] The level of silicon incorporation is defined as the ratio of atomic fraction of Si in the solid respect to the gel: $[Si/(Si + Al + P)]_{solid}/[Si/(Si + Al + P)]_{gel}$

[b] Acid sites concentration determined from ammonia TPD

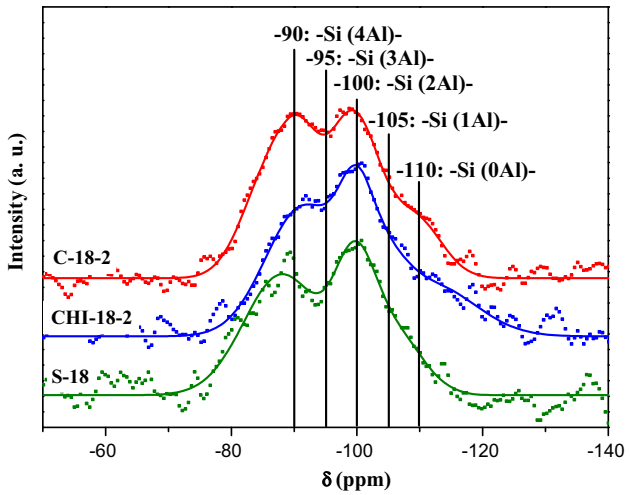

Fig. 8 ^{29}Si CP/MAS NMR spectra of calcined samples

several resonances due to the different Si(nAl) environments ($n = 0$–4), in which the Si atoms are tetrahedrally coordinated to oxygen atoms and surrounded by n Al and 4-n Si atoms in the second coordination sphere. These resonances appear at ca. −90, −95, −100, −105 and −110 ppm, which correspond to Si(4Al), Si(3Al), Si(2Al), Si(Al) and Si(0Al), respectively. The presence of these signals indicates that silicon incorporation occurs by a combination of substitution mechanisms SM2 (substitution of one P atom by a Si atom in the AlPO framework) and SM3 (a simultaneous substitution of a pair Al-P by two Si atoms). Depending on the ratio of SM3 to SM2 substitutions, the size and concentration of the Si islands will be different [58–60]. Some authors have proposed that the strength of the acid sites generated at the border of the Si islands is higher than that of the acid sites created by the isolated Si atoms [Si(4Al) species], and that the strength increases as the value of n in the $Si(OAl)_n(OSi)_{4-n}$ environments decreases [57]. Thus, a higher number of acid sites are generated through the SM2 mechanism, while substitution via SM2 + SM3 yields less but stronger acid sites. The incorporation of Si through the different mechanisms would therefore modulate the acidity of these materials, which would affect catalytic behaviour. The spectra show that in all the samples the predominant environments are Si(4Al) and Si(2Al). Therefore, these materials possess isolated Si atoms and very small silica domains, but no large silicon islands. Chemical analysis

and NMR spectra show that both silicon content and distribution of Si species are similar for all samples, which suggests that they would also possess comparable acid properties. Indeed, ammonia TPD measurements showed closed values for the concentration of acid sites among samples that correlate well with the small variations in total silicon content (Table 4).

3.2 Catalytic Activity

The catalytic activity of these materials in the MTO reaction was evaluated at 673 and 723 K and a WHSV of 1.2 h^{-1}. The time profiles obtained for conversion are plotted in Fig. 9 left, which shows that only samples co-templated with chitosan exhibited a significant increase of catalyst lifetime. It can be seen also that increasing the reaction temperature from 673 to 723 K decreases lifetime and lessens the differences in catalytic activity among the different SAPO-18 samples. In order to compare the activity behaviour of the different catalysts, the data have been fitted using the kinetic model proposed by Janssens [61]. This model was developed to describe the deactivation behaviour of ZSM-5 catalysts in the methanol-to-hydrocarbon reaction. It assumes a first order reaction rate and a non-selective deactivation proportional to the conversion, i.e., that the different hydrocarbon products are formed through a series of consecutive reaction steps that have the same deactivation rate. According to this model, the progress of the deactivation front through the catalyst bed leads to a decrease of the effective contact time, as the mass of active catalyst decreases. Thus, if contact time (τ) is defined as the ration between the mass of (active) catalyst and the molar flow of methanol, the deactivation rate (r_D), in grams of deactivated catalyst per mole of methanol fed can be calculated as:

$$r_D = -\frac{d\tau}{dt} = aX$$

assuming that the deactivation rate is proportional to methanol conversion (X) and has a deactivation constant a.

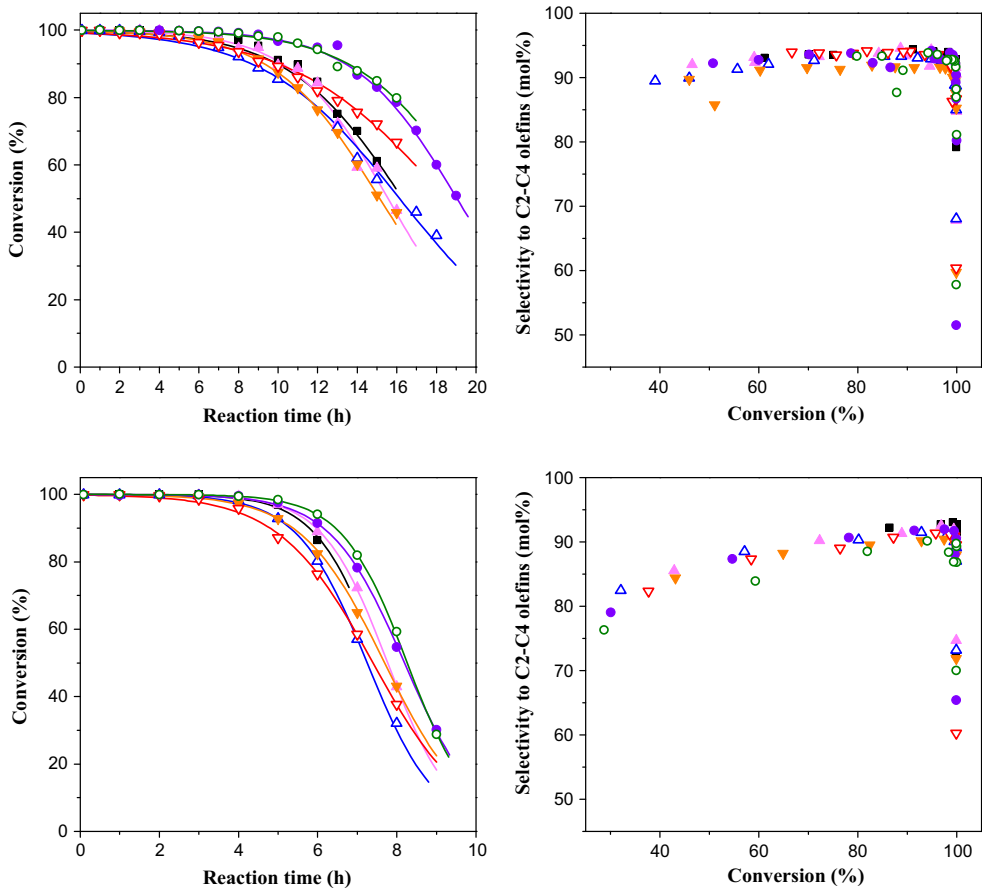

Fig. 9 Conversion as a function of time on stream (*left*) and selectivity to short chain olefins versus conversion (*right*) in the MTO reaction at 673 (*top*) and 723 K (*bottom*). Catalysts: S-18 (*squares*), C-18-1 (*full*, *up triangles*), C-18-2 (*open*, *up triangles*), C-18-1OX (*full*, *down triangles*), C-18-2OX (*open*, *down triangles*), CHI-18-1 (*full circles*) and CHI-18-2 (*open circles*). *Lines* correspond to the fitting of activity data to the kinetic model developed by Janssens [61]

For a first-order reaction with rate constant k, the change of conversion with time is:

$$\frac{dX}{dt} = k(1 - X)$$

and, taking into account the relation between contact time and conversion, the conversion as a function of time-on-stream (t) becomes:

$$X = \frac{(\exp(k\tau_0) - 1)\exp(-kat)}{1 + (\exp(k\tau_0) - 1)\exp(-kat)}$$

where τ_0 is the initial contact time, i.e., the ratio between total amount of fresh catalyst and methanol molar flow rate. Thus, this model allows to describe the catalytic behaviour using two parameters, namely the first order kinetic constant (k) and the deactivation constant (a).

Even though it has been reported that the MTO reaction on SAPO-34 shows a selective deactivation [62], Janssens's kinetic model has been proven to fit well the deactivation profiles of large as well as small nano-crystalline SAPO-34 catalysts [26]. As shown in Fig. 9, this model also fits well the combined methanol and dimethyl ether conversion profiles obtained for SAPO-18 catalysts, at least for conversion levels higher than 30 %. Table 5 summarizes the values obtained for the first order kinetic constant (k) and the deactivation constant (a) for all the tested catalysts, as well as the half lifetime ($t_{0.5}$), i.e., the time to reach 50 % conversion, and the corresponding methanol conversion capacity (R_0), i.e., the maximum amount of methanol that can be converted per unit mass of catalyst before deactivation of the whole catalyst bed, which are derived from k and a [61]:

$$t_{0.5} = \frac{\ln(\exp(k\tau_0) - 1)}{ka}$$

$$R_0 = WHSV_{MeOH} t_{0.5}$$

where $WHSV_{MeOH}$ is the methanol WHSV.

It can be observed that, at a reaction temperature of 673 K, the conversion profiles of the SAPO-18 sample obtained without mesoporogen agents and those synthesized with carbon co-templates are almost coincident and, therefore, their calculated kinetic parameters are also very close. It has been shown [35] that coke formation near the external surface of SAPO crystals gradually blocks the diffusion path of oxygenates to the inner core of the catalysts. As a consequence, even though acid sites are distributed homogenously throughout the crystal, only the outer part of the crystal is effectively involved in the MTO conversion. Therefore, as similar rate constants are calculated for all those samples, this suggests that they possess comparable amount of active sites near the external surface. Taking into account that they possess similar acid sites content and crystal size, this result would support the conclusion that most of the additional mesoporosity generated by using carbon as co-template are intracrystalline mesopores that do not extend to the crystal surface and, therefore, do not enhance accessibility to micropores. Only the sample synthesized with the largest amount of pre-oxidized carbon (C-18-2OX) shows a small increase of lifetime (a half lifetime of 18.5 h compared to 15–16 h) and conversion capacity (from ca. 19 to 22 g of methanol per gram of catalyst), due to its slower deactivation rate. At higher reaction temperature (723 K), all the catalysts show a substantial decrease of lifetime and conversion capacity (Table 5). The

Table 5 Rate constant, deactivation coefficient, half lifetime and methanol conversion capacity calculated for the SAPO-18 catalysts

Temperature (K)	Sample	k (mol/g_{cat} h)	a (mg_{cat}/mol)	$t_{0.5}$ (h)	R_0 (g_{MeOH}/g_{cat})
673	S-18	5.6	61	16.3	19.6
	C-18-1	6.4	64	15.6	18.7
	C-18-2	4.7	62	16.1	19.4
	C-18-1OX	5.7	66	15.1	18.1
	C-18-2OX	4.8	54	18.5	22.2
	CHI-18-1	7.4	53	19.1	22.9
	CHI-18-2	6.9	50	19.9	23.8
723	S-18	9.3	132	7.6	9.1
	C-18-1	9.5	129	7.8	9.3
	C-18-2	8.2	138	7.3	8.7
	C-18-1OX	7.3	130	7.7	9.2
	C-18-2OX	6.3	135	7.4	8.8
	CHI-18-1	8.8	122	8.2	9.8
	CHI-18-2	10.0	121	8.3	9.9

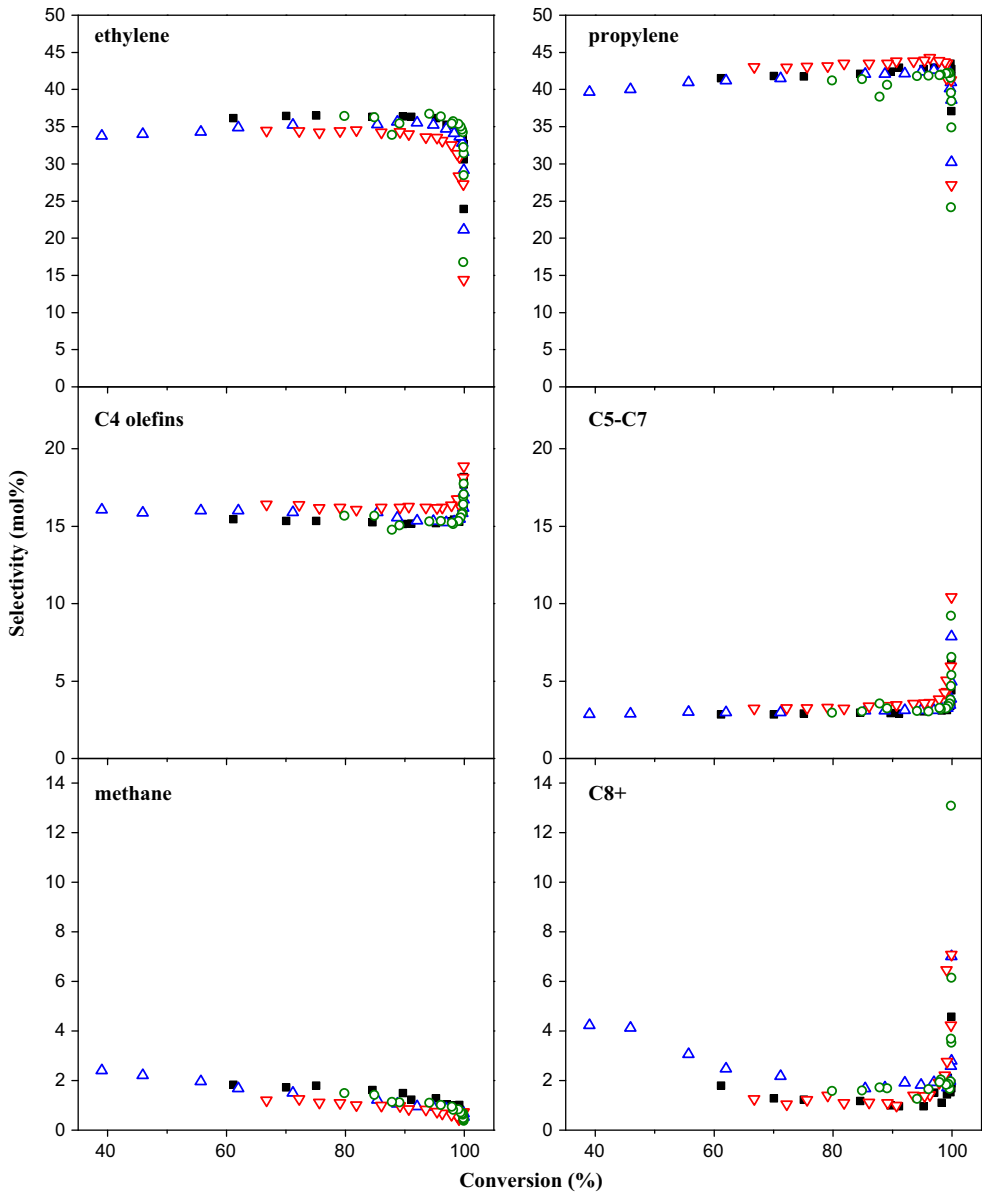

Fig. 10 Product selectivities versus conversion in the MTO reaction at 673 K. Catalysts: S-18 (*squares*), C-18-2 (*up triangles*), C-18-2OX (*down triangles*) and CHI-18-2 (*circles*)

kinetic constants calculated at this temperature are notably higher than those obtained at 673 K, indicating a higher overall rate of conversion of methanol. However, this effect seems to be overcompensated by a large increase of the deactivation rate, as the deactivation constants increase by more than a factor 2. These data suggest that at the higher temperature the rate of coke deposition increases, which enhances the pore blocking that causes catalyst deactivation. At 723 K, all the catalysts obtained with carbon co-template show lifetime and conversion capacity values very close to those of the SAPO-18 sample synthesized without co-template. In contrast, samples prepared with chitosan show a small but meaningful enhancement of lifetime and conversion capacity at both reaction temperatures, which increase with the amount of additive. For these samples, higher rate constants and lower deactivation coefficients are obtained, which suggests that the addition of chitosan to the synthesis gels leads to SAPO-18 crystals with enhanced accessibility of micropores and, therefore, improved mass transport of reactants and products.

All the materials prepared show similar selectivities to the different reaction products at the same conversion level, with ethylene and propylene as the main products followed by C4 olefins (Fig. 10 and Fig. S2, Supplementary Information). Therefore, the introduction of mesopores does not change the product formation significantly. At the

start of the reaction, when the conversion level is close to 100 %, as the catalyst deactivation front moves downstream, the rate of the consecutive reactions that transform ethylene and propylene into heavier products on the fresh catalyst decreases due to the decrease of the effective residence time. Thus, during the initial reaction period, at 100 % conversion, selectivities to ethylene and propylene increase and selectivities to heavier products decrease with time. Selectivities to the different products reach a nearly constant level once the conversion start to decrease until it reaches nearly 50 %. At lower conversion levels, ethylene and propylene selectivities start to decrease while selectivity to aromatics (C8+) increases together with methane, which production remains nevertheless at low levels with small increase along the whole reaction test.

At 673 K, all the catalysts exhibited the same variation of selectivity to light olefins (C2–C4) with conversion (Fig. 9, right). After the initial increase of the selectivity while conversion is 100 %, selectivity to light olefins reaches ca. 92 %, and this value remains nearly constant as conversion decreases from 100 to 60 %. At lower conversion levels, selectivity shows a slight decrease with conversion. Under these conditions, the ethylene/propylene molar ratio obtained is close to 0.8 and shows a continuous slight increase with reaction time (Fig. S3, Supplementary Information). At 723 K, the decrease of light olefins selectivity with conversion is more pronounced and shows an almost linear decay from 90 % at conversion close to 100 to 85 % for a conversion level around 50 %. Furthermore, higher ethylene/propylene molar ratio is obtained (around 1.0–1.2) at 723 K. The raise in ethylene/propylene ratio with temperature has been previously attributed to the secondary reactions of oligomerization and cracking, which are favoured when the reaction temperature increases [17, 63].

From the results presented here, it can be concluded that the increase of external or mesoporous surface of SAPO-18 catalysts would be an important parameter to control the catalytic behaviour in order to obtain more stable materials with longer lifetime. All the materials prepared in this work presented similar framework composition, silicon distribution and acidity, and the main difference among them is the hierarchical porosity generated. An introduction of chitosan polymer as a secondary template results in an increase of the non-micropore to micropore surfaces ratio, which improved significantly the internal diffusivity enhancing the life time of the catalyst in the MTO process.

4 Conclusions

SAPO-18 catalysts have been synthesized using carbon nanoparticles and chitosan as secondary templates. Chitosan rendered mesopore-modified SAPOs with higher external surface which improved significantly the internal diffusivity of these materials. This increase in the network mesoporosity is an important factor allowing to obtain materials with improved catalytic performance in the MTO process, which retain high conversion level for longer reaction time compared with the conventional material.

Acknowledgments We are thankful for the financial support of the Spanish Ministry of Economy and Competitiveness, Project MAT2012-31127.

References

1. Olah GA, Goeppert A, Prakash GKS (2009) Chemical recycling of carbon dioxide to methanol and dimethyl ether: from greenhouse gas to renewable, environmentally carbon neutral fuels and synthetic hydrocarbons. J Org Chem 74(2):487–498
2. Song C (2006) Global challenges and strategies for control, conversion and utilization of CO_2 for sustainable development involving energy, catalysis, adsorption and chemical processing. Catal Today 115(1–4):2–32
3. Hamelinck CN, Faaji APC (2002) Future prospects for production of methanol and hydrogen from biomass. J Power Sour 111:1–22
4. Chang CD (1984) Methanol conversion to light olefins. Catal Rev 26(3–4):323–345
5. Chang CD, Silvestri AJ (1977) The conversion of methanol and other O-compounds to hydrocarbons over zeolite catalysts. J Catal 47:249–259
6. Chang CD, Silvestri AJ (1987) MTG: origin, evolution, operation. ChemTech 17:624–631
7. Chang CD, Silvestri AJ, Smith RL (1975) Aromatization reactions U. S. Patent 3(894):103
8. Kaeding WW, Butter SA (1980) Production of chemicals from methanol: I. Low molecular weight olefins. J Catal 61(1): 155–164
9. Chang CD (1983) Hydrocarbons from methanol. Catal Rev 25(1):1–118
10. Inui T, Medhanavyn D, Praserthdam P, Fukuda Takayo K, Akira Sakamoto U, Miyamoto A (1985) Methanol conversion to hydrocarbons on novel vanadosilicate catalysts. Appl Catal 18(2):311–324
11. Inui T, Miyamoto A, Matsuda H, Nagata H, Makino Y, Fukuda K, Okazumi F (1986) Stud Surf Sci Catal 28:859–866
12. Howden MG (1985) Zeolite ZSM-5 containing boron instead of aluminium atoms in the framework. Zeolites 5(5):334–338
13. Martin A, Nowak S, Lücke B, Wieker W, Fahlke B (1990) Coupled conversion of methanol and C4-hydrocarbons (CMHC) on iron-containing ZSM-5 type zeolites. Appl Catal 57(1): 203–214
14. Luk'yanov DB (1992) Effect of SiO2Al2O3 ratio on the activity of HZSM-5 zeolites in the different steps of methanol conversion to hydrocarbons. Zeolites 12(3):287–291
15. Gayubo AG, Benito PL, Aguayo AT, Olazar M, Bilbao J (1996) Relationship between surface acidity and activity of catalysts in the transformation of methanol into hydrocarbons. J Chem Technol Biotechnol 65(2):186–192
16. Lok BM, Messina CA, Patton RL, Gajek RT, Cannan TR, Flanigen EM (1984) Silicoaluminophosphate molecular sieves: another new class of microporous crystalline inorganic solids. J Am Chem Soc 106:6092–6093

17. Popova M, Minchev C, Kanazirev V (1998) Methanol conversion to light alkenes over SAPO-34 molecular sieves synthesized using various sources os silicon and aluminium. Appl Catal A 169:227–235
18. Chen D, Moljord K, Fuglerud T, Holmen A (1999) The effect of crystal size of SAPO-34 on the selectivity and deactivation of the MTO reaction. Microporous Mesoporous Mater 29:191–203
19. Zhu Z, Hartmann M, Kevan L (2000) Catalytic conversion of methanol to olefins on SAPO-n (n = 11, 34, and 35), CrAPSO-n, and Cr-SAPO-n molecular sieves. Chem Mater 12:2781–2787
20. Álvaro-Muñoz T, Márquez-Álvarez C, Sastre E (2012) Use of different templates on SAPO-34 synthesis: effect on the acidity and catalytic activity in the MTO reaction. Catal Today 179(1):27–34
21. Álvaro-Muñoz T, Márquez-Álvarez C, Sastre E (2013) Effect of silicon content on the catalytic behavior of chabazite type silicoaluminophosphate in the transformation of methanol to short chain olefins. Catal Today 213:219–225
22. Álvaro-Muñoz T, Márquez-Álvarez C, Sastre E (2013) Enhanced stability in the methanol-to-olefins process shown by SAPO-34 catalysts synthesized in biphasic medium. Catal Today 215:208–215
23. Álvaro-Muñoz T, Márquez-Álvarez C, Sastre E (2014) Aluminium chloride: a new aluminium source to prepare SAPO-34 catalysts with enhanced stability in the MTO process. Appl Catal A 472:72–79
24. Liang J, Li H, Zhao S, Guo W, Wang R, Ying M (1990) Characteristics and performance of SAPO-34 catalyst for methanol-to-olefin conversion. Appl Catal 64:31–40
25. Stöcker M (1999) Methanol-to-hydrocarbons: catalytic materials and their behavior. Microporous Mesoporous Mater 29:3–48
26. Li Z, Martinez-Triguero J, Concepcion P, Yu J, Corma A (2013) Methanol to olefins: activity and stability of nanosized SAPO-34 molecular sieves and control of selectivity by silicon distribution. Phys Chem Chem Phys 15(35):14670–14680
27. Salmasi M, Fatemi S, Taheri Najafabadi A (2011) Improvement of light olefins selectivity and catalyst lifetime in MTO reaction; using Ni and Mg-modified SAPO-34 synthesized by combination of two templates. J Ind Eng Chem 17(4):755–761
28. Álvaro-Muñoz T, Sastre E, Márquez-Álvarez C (2014) Microwave-assisted synthesis of plate-like SAPO-34 nanocrystals with increased catalyst lifetime in the methanol-to-olefin reaction. Catal Sci Technol 4:4330–4339
29. Simmen A, McCusker LB, Baerlocher C, Meier WM (1991) The structure determination and Rietveld refinement of the aluminophosphate AlPO-18. Zeolites 11:654–661
30. Hinsen W, Bytyn W, Baerns M (1984) Paper presented at the Proceedings of the 8th International Congress on Catalysis, Berlin
31. Chen J, Wright PA, Thomas JM, Natarajan S, Marchese L, Bradley SM, Sankar G, Catlow CRA, Gal-Boyes PL, Townsend RP, Lok CM (1994) SAPO-18 catalysts and their Brönsted acid sites. J Phys Chem 98:10216–10224
32. Wendelbo R, Akporiaye D, Andersen A, Dahl IM, Mostad HB (1996) Synthesis, characterization and catalytic testing of SAPO-18, MgAPO-18, and ZnAPO-18 in the MTO reaction. Appl Catal A 142(2):L197–L207
33. Gayubo AG, Aguayo AT, Alonso A, Bilbao J (2007) Kinetic modeling of the methanol-to-olefins process on a silicoaluminophosphate (SAPO-18) catalyst by considering deactivation and the formation of individual olefins. Ind Eng Chem Res 46(7):1981–1989
34. Wilson S, Barger P (1999) The characteristics of SAPO-34 which influence the conversion of methanol to light olefin. Microporous Mesoporous Mater 29:117–126
35. Chen D, Moljord K, Holmen A (2012) A methanol to olefins review: diffusion, coke formation and deactivation on SAPO type catalysts. Microporous Mesoporous Mater 164:239–250
36. Tao YS, Kanoh H, Abrams L, Kaneko K (2006) Mesopore-modified zeolites: preparation, characterization, and applications. Chem Rev 106(3):896–910
37. van Donk S, Janssen AH, Bitter JH, de Jong KP (2003) Generation, characterization, and impact of mesopores in zeolite catalysts. Catal Rev 45(2):297–319
38. Groen JC, Moulijn JA, Perez-Ramirez J (2006) Desilication: on the controlled generation of mesoporosity in MFI zeolites. J Mater Chem 16(22):2121–2131
39. Groen JC, Peffer LAA, Moulijn JA, Pérez-Ramírez J (2005) Mechanism of hierarchical porosity development in MFI zeolites by desilication: the role of aluminium as a pore-directing agent. Chem Eur J 11(17):4983–4994
40. Holland BT, Abrams L, Stein A (1999) Dual templating of macroporous silicates with zeolitic microporous frameworks. J Am Chem Soc 121:4308–4309
41. Jacobsen CJH, Madsen C, Houzvicka J, Schmidt I, Carlsson A (2000) Mesoporous zeolite single crystals. J Am Chem Soc 122:7116–7117
42. Kustova MY, Hasselriis P, Christensen CH (2004) Mesoporous MEL: type zeolite single crystal catalysts. Catal Lett 96(3–4): 205–211
43. Kustova M, Egeblad K, Christensen CH, Kustov AL, Christensen CH (2007) Hierarchical zeolites: progress on synthesis and characterization of mesoporous zeolite single crystal catalysts. Stud Surf Sci Catal 170(A):267–275
44. Wei X, Smirniotis PG (2006) Synthesis and characterization of mesoporous ZSM-12 by using carbon particles. Microporous Mesoporous Mater 89(1–3):170–178
45. Tao Y, Kanoh H, Kaneko K (2003) Uniform mesopore-donated zeolite Y using carbon aerogel templating. J Phys Chem B 107:10974–10976
46. Egeblad K, Kustova M, Klitgaard SK, Zhu K, Christensen CH (2007) Mesoporous zeolite and zeotype single crystals synthesized in fluoride media. Microporous Mesoporous Mater 101(1–2):214–223
47. Kustova M, Egeblad K, Zhu K, Christensen CH (2007) Versatile route to zeolite single crystals with controlled mesoporosity: in situ sugar decomposition for templating of hierarchical zeolites. Chem Mater 19(12):2915–2917
48. Schmidt F, Paasch S, Brunner E, Kaskel S (2012) Carbon templated SAPO-34 with improved adsorption kinetics and catalytic performance in the MTO-reaction. Microporous Mesoporous Mater 164:214–221
49. Fajardo HV, Martins AO, de Almeida RM, Noda LK, Probst LFD, Carreño NLV, Valentini A (2005) Synthesis of mesoporous Al2O3 macrospheres using the biopolymer chitosan as a template: a novel active catalyst system for CO2 reforming of methane. Mater Lett 59(29–30):3963–3967
50. Witoon T, Chareonpanich M, Limtrakul J (2008) Synthesis of bimodal porous silica from rice husk ash via sol–gel process using chitosan as template. Mater Lett 62(10–11):1476–1479
51. Hidrobo A, Retuert J, Araya P (2003) Stable zeolite-containing mesoporous aluminosilicates. J Porous Mater 10:231–234
52. Braga TP, Gomes ECC, Sousa AFd, Carreño NLV, Longhinotti E, Valentini A (2009) Synthesis of hybrid mesoporous spheres using the chitosan as template. J NonCryst Solids 355(14–15): 860–866
53. Dubois V, Dal Y, Jannes G (2002) Active carbon surface oxidation to optimize the support functionality and metallic dispersion of a Pd/C catalyst. Stud Surf Sci Catal 143:993–1002

54. He H, Klinowski J (1993) Solid-state NMR studies of the aluminophosphate molecular sieve $AlPO_4$-18. J Phys Chem 97(40):10385–10388
55. Buchholz A, Wang W, Arnold A, Xu M, Hunger M (2003) Successive steps of hydration and dehydration of silicoaluminophosphates H-SAPO-34 and H-SAPO-37 investigated by in situ CF MAS NMR spectroscopy. Microporous Mesoporous Mater 57(2):157–168
56. Christensen CH, Schmidt I, Carlsson A, Johannsen K, Herbst K (2005) Crystals in crystalsnanocrystals within mesoporous zeolite single crystals. J Am Chem Soc 127(22):8098–8102
57. Janssen AH, Schmidt I, Jacobsen CJH, Koster AJ, de Jong KP (2003) Exploratory study of mesopore templating with carbon during zeolite synthesis. Microporous Mesoporous Mater 65(1): 59–75
58. del Val S, Blasco T, Sastre E, Pérez-Pariente J (1995) Synthesis of SiVPI-5 with enhanced activity in acid catalysed reactions. J Chem Soc Chem Commun 7:731–732
59. Martens JA, Janssens C, Grobet PJ, Beyer HK, Jacobs PA (1989) Stud Surf Sci Catal 49:215–225
60. Prakash AM, Unnikrishnan S, Rao KV (1994) Synthesis and characterization of silicon-rich SAPO-44 molecular sieves. Appl Catal A 110:1–10
61. Janssens TVW (2009) A new approach to the modeling of deactivation in the conversion of methanol on zeolite catalysts. J Catal 264(2):130–137
62. Chen D, Rebo HP, Moljord K, Holmen A (1999) Methanol conversion to light olefins over SAPO-34. Sorption, diffusion, and catalytic reactions. Ind Eng Chem Res 38(11):4241–4249
63. Wu X, Abraha MG, Anthony RG (2004) Methanol conversion on SAPO-34: reaction condition for fixed-bed reactor. Appl Catal A 260(1):63–69
64. Baerlocher Ch, McCusker LB (2001) Database of zeolite structures. http://www.iza-structure.org/databases/. Accessed 3 Aug 2015